IEEE Access
Multidisciplinary ⋮ Rapid Review ⋮ Open Access Journal

Received 9 December 2022, accepted 26 December 2022, date of publication 1 February 2023, date of current version 10 February 2023.

Digital Object Identifier 10.1109/ACCESS.2023.3241593

RESEARCH ARTICLE

Impact of Heat Pumps, Rooftop PV, and Hydrogen Blending on Gas-Electricity Distribution Networks in Northeast US

JONTE DANCKER[1], PABLO DUENAS MARTINEZ[2,3], AND MARTIN WOLTER[1], (Senior Member, IEEE)

[1]Institute of Electric Power Systems, Otto von Guericke University, 39106 Magdeburg, Germany
[2]School of Engineering (ICAI), Institute for Research in Technology, Universidad Pontificia Comillas, 28015 Madrid, Spain
[3]MIT Energy Initiative, Massachusetts Institute of Technology, Cambridge, MA 02139, USA

Corresponding author: Jonte Dancker (jonte.dancker@ovgu.de)

This work was supported in part by the German Research Foundation (DFG) under Grant WO2172/3-1, and in part by the Open Access Publication Fund for Book Processing Charge by Magdeburg University.

ABSTRACT The building sector is responsible for about 7 % of overall greenhouse gas emissions in the US. Cutting the emissions by electrifying heating and cooling supply through heat pumps (HPs) leads to an increase in electricity demand and potential overloading of lines and transformers in electricity distribution systems. Although many studies investigate the maximum potential for HPs in existing distribution systems in Europe, they neglect a potential relieving effect of combining HPs with rooftop photovoltaic (PV) systems as well as the consequence of coupling the electricity and gas system at distribution level. Hence, we investigate the effect of HPs and rooftop PV systems in a representative distribution system in Northeast US and the potential of coupling electricity and gas distribution systems. We show that generally no overloading in average US electric distribution systems occurs even under high realistic HP and PV adoption rates, 40 % and 26 % respectively. Moreover, our results show that combining HPs and rooftop PV reduces the impact on the distribution system throughout the year with the greatest reduction in spring and fall. In contrast, the potential for injecting hydrogen on distribution level is technically very limited and not economic. Under a 20 vol.-% blending strategy, CO_2 emissions would barely decrease 7 %, while energy costs would skyrocket due to the high cost of producing green hydrogen from electrolysis against blue hydrogen from steam methane reforming. Moreover, electrolyzers (ELZs) at distribution level are neither able nor needed to reduce congestion in the electricity system.

INDEX TERMS Distribution system, heat pump, hydrogen injection, integrated energy system, synthetic networks, sector coupling.

I. INTRODUCTION

As society, we need to act on several fronts to mitigate climate change. Most of major emitters, including China, the US, the EU, India, Russia, Japan, and Canada, have pledged or approved legislation to reach net zero emissions by 2050, 2060 or 2070 [1]. To reach this goal the power generation, industry, transportation, and building sectors must be decarbonized. A strong focus is set on the building sector as the sector represented about 10 % of direct CO_2 emissions in 2020 [2]. Major CO_2 emission reductions are expected by implementing energy efficiency measures and electrifying heating and cooling loads through heat pumps (HPs).

Looking at the US, space heating of buildings is responsible for about 7 % of overall greenhouse gas emissions [3]. Mitigating these emissions by electrifying fossil-fuel-based heating in buildings will affect the operation of distribution

The associate editor coordinating the review of this manuscript and approving it for publication was Diego Bellan.

networks, e. g., increase in peak load, increase in non-coincident peak load by 70 %, switch from summer to winter peaking [4].

A study of a generic network in the UK showed that substation transformers may be overloaded when HP penetration exceeds 20 % while voltage limits remain in limits until 37 % [5]. Another study on low-voltage distribution networks in the UK with different topologies and buildings revealed that old houses (i. e., poorly isolated) only allowed 20 % HP penetration before leading to congestion in the network while modern isolated houses allowed up to 40 % penetration [6]. Similar results are shown by [7] for Belgian low voltage networks. Weak feeders only allowed 20 % to 30 % HP penetration while stronger feeders accommodate 40 % penetration. To reduce the impact on the network and avoid capacity upgrades of the electric power system (EPS) in areas with older houses or cold climate, [8] suggests to use hybrid systems. Although the studies where conducted for different European countries all tend to establish a threshold between 20 % to 40 % depending on the building stock and distribution network.

However, distribution systems do not only face an increase in HPs but also an increase in rooftop photovoltaic (PV), which is neglected by the studies. As the combination of HPs and PVs might be beneficial from a network standpoint, the threshold of HPs might be higher than in the above-mentioned studies. Furthermore, as the studies focus on European distribution networks, their results might not be applicable to US networks due to different structures and topologies.

Hence, we investigate the impact of combining HPs and rooftop PV systems on US distribution networks. For this, we select a representative distribution network from a database of realistic synthetic distribution networks [9] and populate it with representative residential and commercial buildings [10], [11] from the Northeast US. With this, we characterize an average behavior of distribution networks and buildings in a cold US climate area. Moreover, we investigate if gas distribution systems can support electric distribution networks by reducing the impact of HPs and PVs through electrolyzers (ELZs) while increasing the renewable energy share in the gas system (GS). With this, the GS would also support a decarbonization of buildings for which HPs are not adoptable either economically or technically, i. e., buildings with weak insulation under very cold weather conditions or high requirements of heat. We investigate the technical and economic potential of blending up to 20 vol.-% hydrogen into gas distribution systems, based on the upper limit concluded by several studies [12], [13], [14], [15]. We do not examine hydrogen as a fossil fuel substitute as it would require a complete costly retrofit of the GS.

Our first contribution is a complete methodological approach. After selecting a representative distribution network in terms of loading, number of consumers, and residential/commercial ratio, we populate this network with representative buildings of a specific climate region. We then run an integrated power and natural gas flow analysis considering different levels of HP and PV penetration, as well as hydrogen production from distributed ELZs, which are connected ex-ante at relevant nodes in the distribution network. This full approach allows us to fill the gap on questions such as the readiness of US distribution networks to accommodate significant levels of HP and rooftop PV systems, the economics of hydrogen blending to reduce CO_2 emissions, and the role of ELZs to alleviate voltage limitations or congestion that may occur from HP and rooftop PV penetration.

To the best of the authors' knowledge, this paper is the first to investigate the joint impact of HPs, rooftop PV systems, and hydrogen blending in a realistic US distribution setup.

The paper continues in Section II formulating the integrated gas-electricity power flow model. We then describe in Section III the case study including the setup, scenarios, power impact and hydrogen behavior, and discuss the results. Finally, we highlight the most relevant conclusions (Section IV).

II. ELECTRICITY-GAS POWER FLOW

A. ELECTRIC POWER SYSTEM

The system state of an EPS is usually determined by a steady-state power flow calculation (e. g., [16], [17], [18], [19]). Assuming a steady-state operation is reasonable as the EPS reaches a steady-state within seconds after a change in system state and thus within a simulation time increment of the power flow calculation, e.g., 15 min. The state of an EPS is described by the complex nodal voltages, which are split into voltage angle $\boldsymbol{\delta}_\mathrm{N}$ and voltage magnitude $\boldsymbol{u}_\mathrm{N}$ in the state vector $\boldsymbol{x}_\mathrm{ps}$ (e. g., [16], [17]):

$$\boldsymbol{x}_\mathrm{ps} = \left[\boldsymbol{\delta}_\mathrm{N}^\mathrm{T}\ \boldsymbol{u}_\mathrm{N}^\mathrm{T}\right]^\mathrm{T} \tag{1}$$

with the voltage magnitude $\boldsymbol{u}_\mathrm{N}$ being pu-values, based on the nominal voltage level of the investigated network U_ref.

The nodal voltage angle and magnitude are determined based on the the active and reactive power flow balances on all nodes except for one slack node:

$$\Delta\boldsymbol{p}_\mathrm{p,N} = \mathrm{Re}\left\{\underline{\boldsymbol{U}}_\mathrm{N}\,\underline{\boldsymbol{Y}}_\mathrm{NN}^*\,\underline{\boldsymbol{u}}_\mathrm{N}^*\right\} - \boldsymbol{p}_\mathrm{p,N,set} = \boldsymbol{0} \tag{2}$$

$$\Delta\boldsymbol{p}_\mathrm{q,N} = \mathrm{Im}\left\{\underline{\boldsymbol{U}}_\mathrm{N}\,\underline{\boldsymbol{Y}}_\mathrm{NN}^*\,\underline{\boldsymbol{u}}_\mathrm{N}^*\right\} - \boldsymbol{p}_\mathrm{q,N,set} = \boldsymbol{0} \tag{3}$$

Here, $\underline{\boldsymbol{U}}_\mathrm{N}$ being a diagonal matrix of the complex nodal voltages $\underline{\boldsymbol{u}}_\mathrm{N}$. The node admittance matrix $\underline{\boldsymbol{Y}}_\mathrm{NN}$ represents the network topology and the equipment characteristics. $\boldsymbol{p}_\mathrm{p,N,set}$ and $\boldsymbol{p}_\mathrm{q,N,set}$ are the pu-values of the known nodal active and reactive power injections or withdrawals (i. e., set points), which are based on a reference value $P_\mathrm{s,ref}$. Both balances are joined in the vector of mismatches $\Delta\boldsymbol{f}_\mathrm{eps}$.

A slack node must be defined with a known voltage magnitude and angle [20] as otherwise the Jacobian matrix is not invertible.

B. GAS SYSTEM

In gas distribution systems, the GS is generally assumed to be steady-state as the gas compressibility has only a small effect due to the small gas volume in pipelines and low pressure levels. However, a hydrogen injection introduces a dynamic behavior due to the hydrogen proagation which must be considered. A detailed description of the gas flow calculation can be found in [21]. The state of a GS is described by the pressure at each node $\boldsymbol{\pi}_{\mathrm{N}}$, the volume flow rate at each terminal of the network at standard conditions $\boldsymbol{q}_{\mathrm{v,n,Te}}$, and the calorific value at each node $\boldsymbol{h}_{\mathrm{o,N}}$. The state vector $\boldsymbol{x}_{\mathrm{gs}}$ is of size $(2\,N + Te) \times 1$:

$$\boldsymbol{x}_{\mathrm{gs}} = \left[\boldsymbol{\pi}_{\mathrm{N}}^{\mathrm{T}}\ \boldsymbol{q}_{\mathrm{v,n,Te}}^{\mathrm{T}}\ \boldsymbol{h}_{\mathrm{o,N}}^{\mathrm{T}}\right]^{\mathrm{T}} \tag{4}$$

The nodal calorific value considers a hydrogen injection and tracks the hydrogen propagation through the network, as done in many studies (e. g., [22], [23], [24]).

The vector of mismatches $\Delta \boldsymbol{f}_{\mathrm{gs}}$ contains the continuity equation $\Delta\overline{\boldsymbol{\pi}}_{\mathrm{L}}$, the momentum equation $\Delta\overline{\boldsymbol{q}}_{\mathrm{v,n,L}}$, the reduced demand/generation calorific value flow rate balance $\Delta\boldsymbol{q}_{\mathrm{ho,n,DG,red}}$, the reduced nodal pressure balance $\Delta\boldsymbol{\pi}_{\mathrm{G,red}}$, the steady-state volume flow rate balance of pressure regulators $\Delta\boldsymbol{q}_{\mathrm{v,n,PR}}$, and the nodal calorific value flow rate balance $\Delta\boldsymbol{q}_{\mathrm{ho,n,N}}$:

$$\begin{aligned}\Delta \boldsymbol{f}_{\mathrm{gs}} = &\begin{bmatrix} \Delta\overline{\boldsymbol{\pi}}_{\mathrm{L}} \\ \Delta\overline{\boldsymbol{q}}_{\mathrm{v,n,L}} \\ \Delta\boldsymbol{q}_{\mathrm{ho,n,DG,red}} \\ \Delta\boldsymbol{\pi}_{\mathrm{G,red}} \\ \Delta\boldsymbol{q}_{\mathrm{v,n,PR}} \\ \Delta\boldsymbol{q}_{\mathrm{ho,n,N}} \end{bmatrix} = \begin{bmatrix} \overline{\boldsymbol{\pi}}_{\mathrm{L,calc}} \\ \overline{\boldsymbol{q}}_{\mathrm{v,n,L,calc}} \\ \boldsymbol{q}_{\mathrm{ho,n,DG,calc}} \\ \boldsymbol{\pi}_{\mathrm{G,red,calc}} \\ \boldsymbol{q}_{\mathrm{v,n,PR,calc}} \\ \boldsymbol{q}_{\mathrm{ho,n,N,calc}} \end{bmatrix} \\ &- \begin{bmatrix} \boldsymbol{0} \\ \boldsymbol{0} \\ \boldsymbol{q}_{\mathrm{ho,n,DG,set}} \\ \boldsymbol{\pi}_{\mathrm{G,red,set}} \\ \boldsymbol{0} \\ \boldsymbol{q}_{\mathrm{ho,n,N,set}} \end{bmatrix}\end{aligned} \tag{5}$$

The first and second balance in (5) determine the terminal volume flow rates under steady-state conditions. For this, the continuity and momentum equation are simplified by assuming a one-dimensional flow, compressible and homogeneous fluid, horizontal pipelines, and an isothermal flow. The simplified equations are discretized by a centered difference scheme in space. Choosing a space discretization equal to the length of the pipeline L leads to:

$$\Delta\overline{\pi}_{l} = \frac{\rho_{\mathrm{n}}\, c^2}{A_l}\,\frac{Q_{\mathrm{v,n,ex}} - Q_{\mathrm{v,n,in}}}{2\,L} = 0 \tag{6}$$

$$\Delta\overline{Q}_{\mathrm{v,n},l} = \frac{\pi_{\mathrm{ex}} - \pi_{\mathrm{in}}}{2\,L} + \frac{\overline{f}_l\,\rho_{\mathrm{n}}^2\,c^2}{2\,D_{\mathrm{i},l}\,A_l\,\overline{\pi}}\,\overline{Q}_{\mathrm{v,n},l}\left|\overline{Q}_{\mathrm{v,n},l}\right| = 0 \tag{7}$$

Here, $\overline{Q}_{\mathrm{v,n},l}$ and $\overline{f}$ are the mean volume flow rate at standard conditions and the mean friction factor of the pipeline, which is flow dependent and determined as in the DHS. ρ_{n} is the gas density at standard conditions while $D_{\mathrm{i},l}$ and A_l are the pipeline's inner diameter and cross-sectional area. As the spatial discretization is equal to the length of the pipeline, the volume flow rates at the inlet and outlet of a pipeline $Q_{\mathrm{v,n,in}}$ and $Q_{\mathrm{v,n,ex}}$ are used. The isothermal speed of sound c is determined by the state equation:

$$c^2 = \frac{\pi}{\rho} = Z\,R\,\vartheta \tag{8}$$

in which R and ϑ are the specific gas constant and gas temperature while the compressibility factor Z is determined by Papay's equation which is also used by [25] and [23]:

$$\begin{aligned}Z = 1 - 3.52\left(\frac{\pi}{\pi_{\mathrm{c}}}\right)\exp\left(-2.260\left(\frac{\vartheta}{\vartheta_{\mathrm{c}}}\right)\right) \\ + 0.274\left(\frac{\pi}{\pi_{\mathrm{c}}}\right)^2\exp\left(-1.878\left(\frac{\vartheta}{\vartheta_{\mathrm{c}}}\right)\right)\end{aligned} \tag{9}$$

in which π_{c} and ϑ_{c} are the pseudo-critical pressure and temperature. The equation is valid for pressures up to 150 bar and natural gas mixtures with up to 20 vol.-% of hydrogen [23]. The gas properties of the gas mixture in each pipeline are determined by averaging the gas properties of hydrogen and natural gas according to their share in the gas mixture.

The third and fourth balance in (5) determine the nodal pressures. The reduced nodal demand/generation calorific value flow rate balance $\Delta\boldsymbol{q}_{\mathrm{ho,n,DG,red}}$ is set up for all nodes, except known pressure nodes (e. g., slack node):

$$\Delta Q_{\mathrm{ho,n},dg,\mathrm{red}} = \sum_{i=1}^{Te} Q_{\mathrm{ho,n},i} - Q_{\mathrm{ho,n},n,\mathrm{set}} = 0 \tag{10}$$

The balance is set up as a calorific value flow rate balance to consider a varying calorific value due to hydrogen injection, ensuring that the energy demand at consumers is met. The pressure balance, on the other hand, is set up for all nodes at which the pressure level is known (e. g., slack node and lower pressure nodes of pressure regulators):

$$\Delta\pi_g = \pi_{g,\mathrm{calc}} - \pi_{g,\mathrm{set}} = 0 \tag{11}$$

The fifth balance in (5) determine the terminal volume flow rates of pressure regulators. In this, we assume a steady-state volume flow rate through a regulator:

$$\Delta Q_{\mathrm{v,n},pr} = Q_{\mathrm{v,n},pr,\mathrm{in}} - Q_{\mathrm{v,n},pr,\mathrm{ex}} = 0 \tag{12}$$

The last balance in (5) determines the nodal calorific value, including the effect of a varying hydrogen share in the GS. The propagation of a change in hydrogen in a GS can be described by a simplified one-dimensional advection partial differential equation (PDE) [22]:

$$\frac{\partial H_{\mathrm{o}}}{\partial t} + \overline{v}\,\frac{\partial H_{\mathrm{o}}}{\partial x} = 0 \tag{13}$$

which can be solved to determine the calorific value at the outlet of a pipeline as:

$$H_{\mathrm{o,ex},\nu} = H_{\mathrm{o,in},\nu-\tau} \tag{14}$$

As no source term is included in (13), the calorific value entering a pipeline reaches the outlet unchanged after a transfer delay τ along the pipeline:

$$\tau = \frac{L}{\overline{v}} \tag{15}$$

If the propagation is assumed to be steady-state (i. e., a change in calorific value occurs simultaneously on all nodes in the network) the transfer delay is zero. The propagation of hydrogen described by (14) and (15) can be included into the power flow calculation by the calorific-value-gradient method described in [21]. With this the calorific value flow rate balance is set up for all nodes except for the slack node, tracking the hydrogen distribution:

$$\begin{aligned}\Delta Q_{\mathrm{ho,n},n} = &\sum H_{\mathrm{o},l,\mathrm{ex}}\, Q_{\mathrm{v,n},l,\mathrm{ex}} \\ &- H_{\mathrm{o},n}\left(-Q_{\mathrm{v,n},n,\mathrm{set}} + \sum Q_{\mathrm{v,n},l,\mathrm{in}}\right) \\ &- Q_{\mathrm{ho,n},n,\mathrm{set}} = 0\end{aligned} \tag{16}$$

The difference between the nodal calorific value flow rate balance and the reduced demand/generation calorific value flow rate balance in (10) lies in the calculation of the calorific value flow rates. While $\Delta \boldsymbol{q}_{\mathrm{ho,n,DG,red}}$ assigns the incoming and leaving volume flow rates the same calorific value (i. e., the nodal calorific value), $\Delta \boldsymbol{q}_{\mathrm{ho,n,N}}$ assigns both flow rates different calorific values. The calorific value flow rate entering the node is determined by the calorific value at the end of the respective edge, while the leaving calorific value flow rate is determined with the calorific value of the node. The calorific value flow rate entering the node is determined by applying the calorific-value-gradient method described in [21] and thus considers the transfer delay of the hydrogen propagation.

C. INTEGRATED ELECTRICITY-GAS POWER FLOW

As in the steady-state power flow calculation of an Integrated Energy System (IES), the equation systems of the different energy systems are joined in a single equation system, resulting in the state vector $\boldsymbol{x}_{\mathrm{ies}}$ and the vector of mismatches $\Delta \boldsymbol{f}_{\mathrm{ies}}$ of the joined power flow calculation:

$$\boldsymbol{x}_{\mathrm{ies}} = \left[\boldsymbol{x}_{\mathrm{ps}}^{\mathrm{T}}\ \boldsymbol{x}_{\mathrm{gs}}^{\mathrm{T}}\right]^{\mathrm{T}} \tag{17}$$

$$\Delta \boldsymbol{f}_{\mathrm{ies}} = \left[\Delta \boldsymbol{f}_{\mathrm{ps}}^{\mathrm{T}}\ \Delta \boldsymbol{f}_{\mathrm{gs}}^{\mathrm{T}}\right]^{\mathrm{T}} \tag{18}$$

To improve the computational efficiency and to reduce convergence issues of the joined power flow calculation, the state variables in (17) are normalized, reducing the order of magnitude of the values in the Jacobian matrix [26]. In the EPS, the voltage magnitude $\boldsymbol{u}_{\mathrm{N}}$ is based on the nominal voltage level U_{ref}. In the GS, the nodal pressures $\boldsymbol{\pi}_{\mathrm{N}}$ and the nodal calorific values $\boldsymbol{h}_{\mathrm{o,N}}$ are related to the nominal pressure level of the network $\pi_{\mathrm{ref,gs}}$ and the calorific value of natural gas $H_{\mathrm{o,ref}}$, respectively.

The Jacobian matrix $\boldsymbol{J}_{\mathrm{ies}}$ is set up based on the derivatives of the vector of mismatches $\Delta \boldsymbol{f}_{\mathrm{ies}}$ with respect to the state vector $\boldsymbol{x}_{\mathrm{ies}}$:

$$\boldsymbol{J}_{\mathrm{ies}} = \begin{bmatrix}\boldsymbol{J}_{\mathrm{ps}} & \boldsymbol{J}_{\mathrm{g2p}} \\ \boldsymbol{J}_{\mathrm{p2g}} & \boldsymbol{J}_{\mathrm{gs}}\end{bmatrix} \tag{19}$$

in which the submatrices on the main diagonal being the Jacobian matrices of the single energy systems. The non-diagonal submatrices, on the other hand, represent the coupling and interdependencies between the two energy systems. Whether a non-diagonal submatrix contains non-zero elements depends on the coupling units in the IES and their operation mode.

The power-to-gas Jacobian matrix $\boldsymbol{J}_{\mathrm{p2g}}$ has non-zero elements if a power-led ELZ is included in the IES:

$$\boldsymbol{J}_{\mathrm{p2g}} = \begin{bmatrix}0 & 0 & \frac{\partial \Delta \boldsymbol{q}_{\mathrm{ho,n,DG,red}}^{\mathrm{T}}}{\partial \boldsymbol{\delta}_{\mathrm{N}}} & 0 & 0 & \frac{\partial \Delta \boldsymbol{q}_{\mathrm{ho,N}}^{\mathrm{T}}}{\partial \boldsymbol{\delta}_{\mathrm{N}}} \\ 0 & 0 & \frac{\partial \Delta \boldsymbol{q}_{\mathrm{ho,n,DG,red}}^{\mathrm{T}}}{\partial \boldsymbol{u}_{\mathrm{N}}} & 0 & 0 & \frac{\partial \Delta \boldsymbol{q}_{\mathrm{ho,N}}^{\mathrm{T}}}{\partial \boldsymbol{u}_{\mathrm{N}}}\end{bmatrix}^{\mathrm{T}} \tag{20}$$

The ELZ affects not only the hydrogen gas infeed, depicted by the derivatives of the reduced demand/generation calorific value flow rate balance $\Delta \boldsymbol{q}_{\mathrm{ho,n,DG,red}}$ but also reduces the calorific value, affecting the nodal calorific value flow rate balance $\Delta \boldsymbol{q}_{\mathrm{ho,N}}$.

The gas-to-power Jacobian matrix $\boldsymbol{J}_{\mathrm{g2p}}$ contains only non-zero elements if an ELZ is operated in gas-led mode:

$$\boldsymbol{J}_{\mathrm{g2p}} = \begin{bmatrix}0 & \frac{\partial \boldsymbol{p}_{\mathrm{p,N}}}{\partial \boldsymbol{q}_{\mathrm{v,n,Te},\nu}^{\mathrm{T}}} & 0 \\ 0 & 0 & 0\end{bmatrix} \tag{21}$$

III. CASE STUDY

A. LOAD, GENERATION, AND NETWORK DATA

We investigate the impact of HP and PV systems and the need and potential of coupling the EPS and GS on distribution level based on a synthetic US MV-level distribution system located in Northeast US.

As no suitable network data for a distribution network in Northeast US is available, we extract a single MV/MV substation, which is representative for most MV/LV sub-networks from a synthetic network representing the San Francisco Bay Area with approx. 2.2 mio. consumers given in [9]. We assume that the network topology and main characteristics of distribution systems in the US are similar for different regions and only the load profiles differ.

To choose a subnetwork for the analysis, all connections between feeders connected to different MV/MV substations are removed, resulting in fully radial systems. The splitting led to substation congestion and nodal voltages below the limit in more than half of the subnetworks for the time step with the highest load using the load data given in the original data. As these subnetworks are not suitable for our analysis, we disregard them. A comparison of the main characteristics of the remaining subnetworks shows that most MV networks are similar in their size, number of connected consumers, and power flow results (see Fig. 1, top and Fig. 2).

The network is adapted to a Northeast US network by replacing the load and generation profiles of all buildings with data of the Swampscott area, MA, USA with a resolution

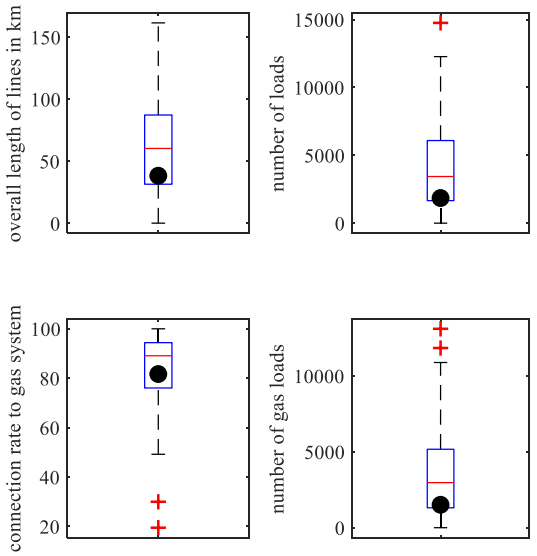

FIGURE 1. Topology characteristics of all MV subnetworks in the data set and the network chosen for the analysis (black dots).

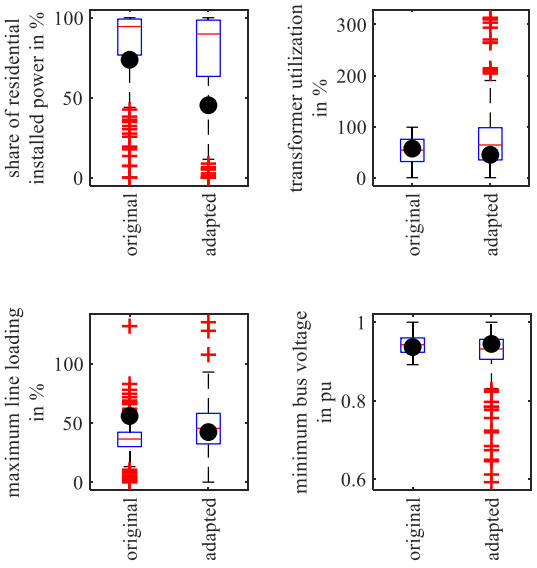

FIGURE 2. Power flow characteristics of MV-networks at time step of highest load. Comparison of original load data with ResStock [11] and ComStock [10] adapted networks.

of 15 min. The residential and commercial load profiles are taken from the ResStock [11] and ComStock [10] building database. The rooftop PV generation profiles are taken from [27], indicating different orientations of the roof, i. e., east, west, and south. The effect of HPs on the load profile is determined by converting the space heating demand, which is given in the ResStock database, to an electricity consumption based on a HPs temperature-dependent coefficient of performance.

The different ResStock and ComStock buildings and their load types are distributed in the network based on their peak power demand, assigning loads to nodes which have a similar peak demand in the original network data set. Comparing the power flow results of the time step with the highest load leads to similar results between the original and adapted load data (see Fig. 2).

TABLE 1. PV and HP adoption scenarios.

Scenario	roof-top-solar	Heat pump
low	no adoption	no adoption
medium[a]	13 % [32]	19 % [33]
high	65 %[b]	40 %[c]

[a]Corresponds to the expected adoption rate by 2030.
[b]Corresponds to the entire use of suitable roof area for PV, which is 26 % of the overall roof area in the US [34], [35]
[c]Corresponds to the expected adoption rate by 2050.

The GS is derived from CIGRE MV-EPS [28] and KERBER LV networks [29]. The CIGRE MV-EPS is also used by [30] to derive a synthetic GS. The network is adapted to reach a higher degree of meshes based on [31], representing a realistic GS.

Based on the identified buildings and their type of heating supply (i. e., gas, oil, or electricity), the connection rate between the EPS and GS is derived (see Fig. 1, bottom). Due to the size of the synthetic gas network, no more than 1850 consumers can be connected to the GS. With this restriction, the chosen EPS contains 1661 residential and 191 commercial loads. The network features a radial topology with four feeders, a nominal voltage of 12.47 kV, an overall line length of 38.4 km and is supplied via a MV/MV transformer with a rating of 16 MVA. Although the network has a comparable small number of loads and overall length of the network (see black dots in Fig. 1), the network represents an average MV network based on the power flow results (see Fig. 2).

In contrast, the GS has two pressure levels of 13 bar and 0.35 bar and two pressure regulators. The line length reaches approx. 64 km. Based on the building types and the EPS, the GS has 1488 consumers, which results in a connection rate between the EPS and GS of approx. 80 %.

The EPS and GS are connected based on their topology, assuming that lines and pipelines lie mostly in parallel. However, the gas supply node and the transformer are placed at different locations. While the gas supply node is located at the outskirts of the network, the substation is located close to the center of the network.

B. SCENARIOS

We investigate the impact of HPs and PV systems and the potential and need for coupling the EPS and GS at distribution level based on three PV and HP adoption scenarios each (see Table 1). These scenarios are combined to investigate the effect of a simultaneous PV and HP adoption. We only apply these scenarios to the residential buildings in the network. The commercial buildings do not change.

The HPs are distributed in the network based on two factors. First buildings which use oil will install a HP then buildings relying on gas. Second, wealthier households will adopt first. To identify wealthier households we assume

that the more energy they consume, the wealthier they are. However, the installation of a HP does not necessarily mean that the oil or gas boiler is replaced. We assume that the HP is only used for heating purposes, while many buildings rely on oil or gas for hot water or cooking. These, however, are not switched to electricity in our analysis.

The PV systems are distributed based on the annual electricity demand. Buildings with a high demand will adopt first, again assuming that wealthier households are prone to be early adopters. The size of the PV system depends on the roof area given in ResStock. As ResStock does not give the orientation of the roof, we assume that on average 40 % of the available roof area can be used for PV systems. With this we account for roofs facing north and that PV panels are installed with a certain distance to the edge of the roof. Based on the available roof area of each building and a nominal power of 300 W per 1.6 m^2 of PV panel area, we derive the nominal power of the PV system. The orientation of the roof is assigned randomly, choosing between an east, west, and south orientation. Based on the orientation, the nominal power is multiplied with the PV generation profiles from [27], resulting in a varying PV generation over the year.

C. EFFECT ON THE EPS

In the base case (no HP and no PV adoption) the substation utilization varies mostly between 10 % and 20 % with a few peaks in the summer due to air condition units, which are mostly below 40 % (see Fig. 3, top left). The network is solely importing electricity from the higher voltage levels. With an increasing HP adoption the substation utilization increases slightly (see Fig. 4). In particular during winter the load increases because of the heating demand (see Fig. 3 and 3, left column). In contrast, if only PV systems are introduced into the system, the network starts to export energy throughout the year during the midday periods (negative values in Fig. 3, top row). Moreover, the substation utilization increases to up to 60 % in the summer and we see a stronger variation than in the base case due to the volatility of the PV generation. The analysis shows that the substation utilization changes much stronger in PV adoption scenarios than in HP adoption scenarios. This is because the adoption rate for HPs is much lower that for PV systems, resulting in strongly differing installed power (approx. 2.7 MW of HPs in the 40% scenario to approx. 36.2 MW PV in the 65 % scenario). The high installed PV power is a result of our assumptions (i. e., available roof area and optimal installation angle) and might be lower in reality. If HPs and PVs are adopted simultaneously the substation utilization is reduced slightly by 2 to 3 % in the winter months compared to the case with only PV systems. The beneficial effect of HP and PV is strongest in the transition periods when HPs are still used and PV generates enough electricity. Our results show that even in high HP and PV adoption scenarios no issues occur on the substation. As we use a network that represents an average US distribution network similar results can be expected for most US MV-level distribution systems.

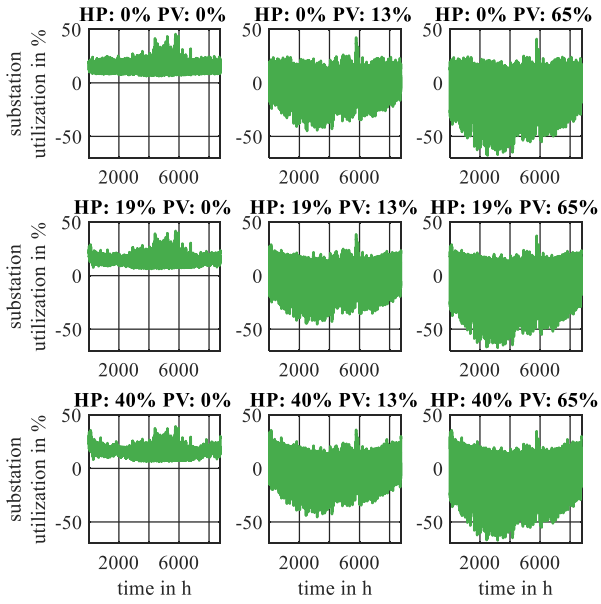

FIGURE 3. Substation utilization during different load and generation scenarios for one year in hourly resolution. A negative utilization indicates an export of energy to the higher voltage level network.

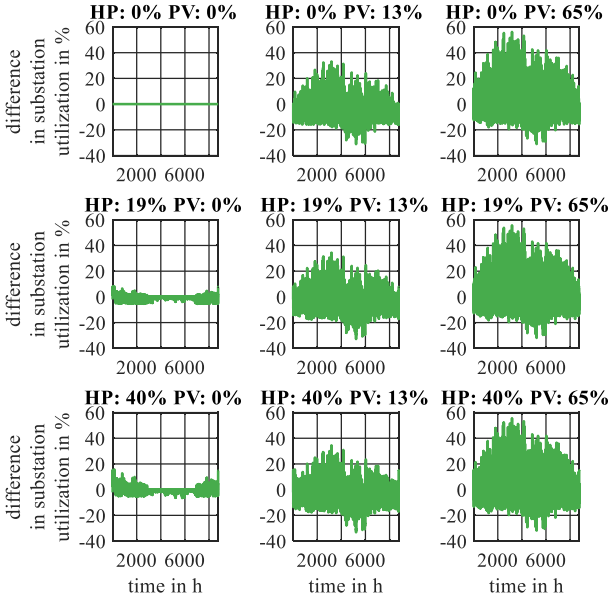

FIGURE 4. Difference of absolute substation utilization compared to the base case (0 % HP, 0 % PV) during different load and generation scenarios for one year in hourly resolution. A negative difference indicates a higher substation utilization in the base case.

Similar to the substation utilization there are no limit violations on lines and nodal voltages in every scenario. However, in six scenarios the utilization of a few lines exceeds 80 %, i. e., HP: 0 % PV: 13 %, HP: 0 % PV: 65 %, HP: 19 % PV: 13 %, HP: 19 % PV: 65 %, HP: 40 % PV: 13 %, HP: 40 % PV: 65 %. The most occurrences happen in scenario HP: 0 % PV: 65 % with 464 hours in which lines are utilized more than 80 % of their rated power. Generally, the issues occur in the high PV scenarios during the midday period in spring and summer when PV generation is the highest and load is generally small.

The high utilization occurs on all feeders and on lines which are close to the substation.

A limit violation, however, only takes place when the PV adoption would reach a level of close to 100 %, meaning that all the roof area is used for PV systems and no margins between the PV panel and edge of the roof are assumed. However, such an adoption is unrealistic as not the entire roof area is suitable for PV systems and a PV system is not economical viable for all buildings.

As we have used a network that represents the average US MV-level distribution system, we conclude that generally no limit violations or congestion happen even for the most optimistic scenarios in terms of HP and PV adoption. Hence, a coupling between the GS and EPS is not needed to support a safe network operation.

D. HYDROGEN INJECTION

In the following, we analyze the potential and effect of three cases for injecting hydrogen into the GS. In the first two cases, a single ELZ is operated so that a constant hydrogen share of 10 % or 20 % is reached in the GS throughout the year. The ELZ operates in a gas-led mode as its operation is determined based on the gas demand. The limits correspond to today's hydrogen limits in the GS and plans of utilities in the US [15]. To maximize the hydrogen injection, the ELZ is placed at the gas supply node of the gas distribution system as here the gas flow is at the highest. In the EPS, the ELZ is connected to a node which is the closest to the gas supply node and which can cope with the additional load.

In the third case, we investigate the potential of injecting hydrogen to reduce peaks during high line utilization, limiting the line utilization to 80 %. As limit violations can occur on multiple locations, multiple ELZs are used in this case. The ELZs operate in a power-led mode as their operation depends on the system state of the EPS. The exact location of the ELZs is determined so that they have the largest impact in the EPS. In the investigated network, the line utilization on three feeders exceeds 80 % in a few hours per year. Hence, three power-led ELZs (i.e., ELZ 1, ELZ 2, ELZ 3) are placed close to the first line in each feeder where a line utilization of over 80 % occurs. Due to the network topology, the ELZs are connected to the low pressure network of the GS close to the gas consumers. The ELZs reduce the line utilization during the hours when the PV generation exceeds the load and the line utilization reaches a level of more than 80 %. The nominal power of the ELZs in the different use cases is shown in Table 2.

In the case of a constant hydrogen injection the potential of the ELZ is higher during the winter season because of a higher gas demand. The potential reduces with a higher HP adoption as less gas is used. However, the potential only reduces for a HP adoption rate of 40 % as in the 19 % scenario mostly buildings that used oil for heating adopt HPs. Thus, there is no effect on the gas demand in the 19 % scenario.

The ELZ increases the network load between 5 and 10 % with peaks of up to 15 % in winter and 3 % in summer if no HPs are introduced. With higher HP scenarios the impact of the ELZ gets smaller as its nominal power is reduced (see Table 2) and the overall network consumption increases due to the utilization of HPs.

TABLE 2. Nominal power of electrolyzers in kW for different load and generation scenarios as well as hydrogen limits.

Scenario	Hydrogen-Case		
	10 vol.-%[a]	20 vol.-%[a]	variable vol.-%[b]
HP: 0 % PV: 0 %	767	1487	0 / 0 / 0
HP: 0 % PV: 13 %	767	1487	82 / 0 / 0
HP: 0 % PV: 65 %	767	1487	438 / 785 / 1215
HP: 19 % PV: 0 %	767	1487	0 / 0 / 0
HP: 19 % PV: 13 %	767	1487	380 / 0 / 0
HP: 19 % PV: 65 %	767	1487	436 / 887 / 907
HP: 40 % PV: 0 %	669	1298	0 / 0 / 0
HP: 40 % PV: 13 %	669	1298	220 / 0 / 0
HP: 40 % PV: 65 %	669	1298	657 / 957 / 966

[a]Single gas-led ELZ connected to gas supply node and single feeder in EPS.
[b]power-led ELZ 1 / ELZ 2 / ELZ 3, each connected to a different feeder in the EPS and GS.

In the case of a constant 10 % hydrogen level, the ELZ increases the line utilization of the feeder it is connected to between 6 and 7 % during winter and approx. 2 % in summer. The effect on the lines is higher during a small HP adoption due to the smaller electric load. In high PV scenarios the ELZ has a relieving effect on the line utilization, reducing the utilization by approx. 2 % during PV peaks. The effect on the substation is minimal. The ELZ increases the substation utilization by about 1 % to 1.5 % during winter and 0.5 % in summer. Again the effect is smaller in the high HP and PV scenarios.

The results in the case of a 20 % hydrogen level are similar only the numbers generally double compared to the 10 % hydrogen case due to the larger ELZ power.

If the ELZs are used to limit the line utilization to 80 % the ELZs are only needed in the high PV adoption scenarios. Nevertheless, they operate in less than 0.8 % of the hours in a year (see Table 3). The ELZs only need to operate in one to two hours per day during noon depending on the scenario (see blue markers in Fig. 5). The number of hours increases during the summer months and decreases during winter. Although the operation times increase with higher PV utilization, an ELZ operation solely to reduce the impact on lines in the EPS is not economic.

Comparing the needed with the potential ELZ power shows that the needed ELZ power is more than 100 times higher than the potential of the GS (see Fig. 5). Here, the needed ELZ power is the power needed to reduce the line utilization in the EPS to 80 % while the potential is determined by a hydrogen level of 20 % at the injection node in the GS.

Even with higher hydrogen levels, the potential would not be sufficient due to the small gas flows at the time steps when the limit violations in the EPS occur, i. e., at midday during spring and summer. Hence, using ELZs to reduce the line utilization in the EPS and injecting the produced hydrogen into the GS distribution system is not viable.

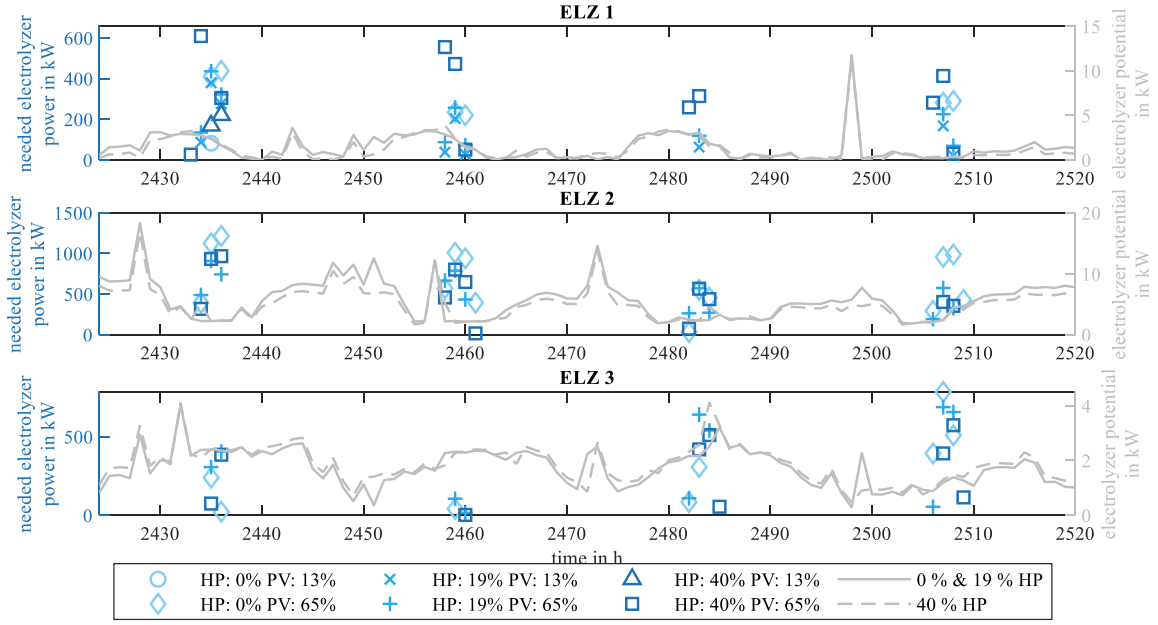

FIGURE 5. Comparison of needed (blue dots, left y-axis) and potential (gray lines, right axis) ELZ power for different load and generation scenarios. The gray lines show how much electric energy the ELZs can maximally convert into hydrogen and inject into the GS without exceeding a hydrogen share of 20 vol.-% in the GS during every hour. The potential of injecting hydrogen depends to the HP adoption rate due to a changing gas consumption. The blue dots show how much electric energy the ELZs would need to convert to limit the line utilization in the EPS to 80 %. The ELZs are mostly switched-off and only operate in the hours which are shown by blue markers. Note the different axis scaling for the needed and potential ELZ power.

TABLE 3. Number of operating hours per ELZ to reduce overloading of 80 % on lines in EPS.

Scenario	ELZ 1	ELZ 2	ELZ 3
HP: 0 % PV: 0 %	0	0	0
HP: 0 % PV: 13 %	2	0	0
HP: 0 % PV: 65 %	18	75	26
HP: 19 % PV: 0 %	0	0	0
HP: 19 % PV: 13 %	14	0	0
HP: 19 % PV: 65 %	24	62	33
HP: 40 % PV: 0 %	0	0	0
HP: 40 % PV: 13 %	4	0	0
HP: 40 % PV: 65 %	52	58	28

E. DISCUSSION

Our results show that on average US distribution systems are oversized. Hence, in contrast to Europe, a higher share of HPs and rooftop PV systems may be introduced without risking congestion. Combining HPs and rooftop PV systems also reduces the impact on the network, reducing generation and consumption peaks. In general and on average, even very optimistic scenarios of HP and PV penetration would not negatively affect the majority of distribution systems in Northeast US.

The potential and impact of hydrogen blending depend on the operation strategy: gas-led or power-led. In the former, the ELZ produces at constant rate to blend hydrogen up to 10 vol.-% and 20 vol.-% into the gas distribution system; while in the latter, the ELZ only produces when locally generated renewable is to be curtailed due to congestion in the EPS.

A gas-led operation mode would allow reducing CO_2 emissions in buildings in which back-up gas boilers are still needed and thus are more difficult to decarbonize. For example in areas where HP performance reduces dramatically due to very cold winter conditions or in badly insulated buildings. For example, [8] estimates that full decarbonization is economically very expensive and it is rational to maintain fossil fuel around 1 – 3 % of heating energy, as backup boilers or furnaces to work during extremely cold days. However, 20 % blending only decreases CO_2 emissions by about only 7 % [14], and it is not clear to be technically feasible as it would still involve meaningful interventions in the GS, such as substituting valves and steel joints, coating or replacing iron-based distribution pipelines, and implementing additional domestic safety measures (e. g., avoiding flash back in burners). A power-led operation mode, on the other hand, is not able to reduce network congestion. Moreover, it is not economic as congestion occur in less than 1 % of the hours in a year.

The potential of combining a gas-led and power-led mode to produce hydrogen at distribution level for residential heating is also economically not reasonable. Producing hydrogen through electrolysis is expected to decrease until 2050 from $ 8.87/kg to $ 5.77/kg when using electricity from the main grid, as in our gas-led ELZ scenario, while the hydrogen production cost would decrease from $ 11.02/kg to $ 5.92/kg when using curtailed (free) electricity, as in our power-led ELZ scenario [36]. Both estimations are still higher than the current cost of producing hydrogen through steam methane reforming at about $ 1.5/kg [37], and whose cost is mainly driven by natural gas prices. This means that hydrogen produced from renewable energies is not

expected to be cost competitive for residential heating against natural gas any time soon. Even less at distribution level and when green hydrogen would be fed by curtailed electricity from distributed renewable resources only leading to an extremely low utilization rate. Moreover, the hydrogen could be used more efficiently for other application, e.g., in the chemical industry, having a greater impact on the overall CO_2-emissions across sectors.

IV. CONCLUSION

Reaching net zero goals demands decisive actions to decarbonize energy uses. A focus is set on the building sector with its approximately 10 % share of global CO_2 emissions. Although technologies such as HPs and hydrogen are available to enable a bottom-up decarbonization, further research is needed on their technical impact on distribution networks, particularly, in the US, and their economics. Therefore, we analyze the impact of HPs, rooftop PV systems, and hydrogen blending in an average US distribution network under cold humid climate conditions, such as Northeast US.

The first conclusion of this study is that distribution feeders are expected to cope with an increasing number of HPs and rooftop PV systems. Even the most promising scenarios of HP penetration by 2050, 40 %, and using all available roof area for PV, 26 %, show a limited impact on voltage limit violations and congestion. We reckon that this conclusion is inferred from a single distribution feeder that is, nevertheless, an average representative of many.

The second conclusion is that blending hydrogen into natural gas may not be rational. First, the reduction in CO_2 is small, 7 %, in comparison to the adaptation effort of natural-gas-oriented pieces and devices. Second, producing hydrogen in ELZs is still expensive and will continue to be more costly than natural gas. To reduce operational cost, ELZs could use curtail (free) electricity while alleviating voltage limit violations and congestion during high PV penetration. On the one hand, such violations only occur in less than 1 % of the hours in a year in an average US distribution system. Thus, the cost reduction effect is too small. On the other hand, the potential to reduce congestion is very small in distribution systems due to small gas flows and hydrogen share limits.

While we have conducted the analysis for a single US distribution system, we contribute a methodological approach for further study of, mainly, more distribution feeders with different configurations in terms of residential/commercial loads, initial utilization level of the substation, and climate conditions. In addition, more ambitious levels of HP penetration are more plausible if federal and state acts and bills pursue an acceleration of achieving net zero goals.

REFERENCES

[1] *Energy & Climate Intelligence Unit | Net Zero Scorecard*, Energy Climate Intell. Unit, London, U.K., 2022. Accessed: Nov. 1, 2022. [Online]. Available: https://eciu.net/netzerotracker

[2] *Net Zero by 2050: A Roadmap for the Global Energy Sector*, Int. Energy Agency, Paris, France, Oct. 2021.

[3] P. Vaishnav and A. M. Fatimah, "The environmental consequences of electrifying space heating," *Environ. Sci. Technol.*, vol. 54, no. 16, pp. 9814–9823, Aug. 2020.

[4] P. R. White, J. D. Rhodes, E. J. H. Wilson, and M. E. Webber, "Quantifying the impact of residential space heating electrification on the Texas electric grid," *Appl. Energy*, vol. 298, Sep. 2021, Art. no. 117113.

[5] M. Akmal, B. Fox, J. D. Morrow, and T. Littler, "Impact of heat pump load on distribution networks," *IET Generation, Transmiss. Distribution*, vol. 8, no. 12, pp. 2065–2073, 2014.

[6] A. Navarro-Espinosa and P. Mancarella, "Probabilistic modeling and assessment of the impact of electric heat pumps on low voltage distribution networks," *Appl. Energy*, vol. 127, pp. 249–266, Aug. 2014.

[7] C. Protopapadaki and D. Saelens, "Heat pump and PV impact on residential low-voltage distribution grids as a function of building and district properties," *Appl. Energy*, vol. 192, pp. 268–281, Apr. 2017.

[8] M. Waite and V. Modi, "Electricity load implications of space heating decarbonization pathways," *Joule*, vol. 4, no. 2, pp. 376–394, Feb. 2020.

[9] *DR POWER | Data Repository for Power System Open Models With Evolving Resources: Bay Area Synthetic Network*, National Renewable Energy Laboratory, Golden, CO, USA, May 2022.

[10] *ComStock—Dataset*, Nat. Renew. Energy Lab., Golden, CO, USA, Jul. 2022.

[11] *ResStock—Dataset*, Nat. Renew. Energy Lab., Golden, CO, USA, Jul. 2022.

[12] M. Melaina, O. Antonia, and M. Penev, "Blending hydrogen into natural gas pipeline networks: A review of key issues," Nat. Renew. Energy Lab., Golden, CO, USA, Tech. Rep. NREL/TP-5600-51995, 2013.

[13] D. Mahajan, K. Tan, T. Venkatesh, P. Kileti, and C. Clayton, "Hydrogen blending in gas pipeline networks—A Review," *Energies*, vol. 15, no. 10, p. 3582, 2022.

[14] J. Bard, N. Gerhardt, P. Selzam, M. Beil, M. Wiemer, and M. Buddensiek, "The limitations of hydrogen blending in the European gas grid," Fraunhofer IEE, Kassel, Germany, Tech. Rep., 2022.

[15] *Hydrogen Blending Impacts Study*, California Public Utilities Commission, San Francisco, CA, USA, 2022.

[16] A. Shabanpour-Haghighi and A. R. Seifi, "An integrated steady-state operation assessment of electrical, natural gas, and district heating networks," *IEEE Trans. Power Syst.*, vol. 31, no. 5, pp. 3636–3647, Sep. 2016.

[17] X. Liu, J. Wu, N. Jenkins, and A. Bagdanavicius, "Combined analysis of electricity and heat networks," *Appl. Energy*, vol. 162, pp. 1238–1250, Jan. 2016.

[18] Z. G. Pan, Q. L. Guo, and H. B. Sun, "Interactions of district electricity and heating systems considering time-scale characteristics based on quasi-steady multi-energy flow," *Appl. Energy*, vol. 167, pp. 230–243, Apr. 2016.

[19] Z. Pan, J. Wu, and M. Abeysekera, "Quasi-dynamic interactions and security control of integrated electricity and heating systems in normal operations," *CSEE J. Power Energy Syst.*, vol. 5, no. 1, pp. 120–129, Mar. 2019.

[20] T. Leveringhaus and L. Hofmann, "Comparison of methods for state prediction: Power flow decomposition (PFD), AC power transfer distribution factors (AC-PTDFs), and power transfer distribution factors (PTDFs)," in *Proc. IEEE PES Asia–Pacific Power Energy Eng. Conf. (APPEEC)*, Dec. 2014, pp. 1–6.

[21] J. Dancker and M. Wolter, "A coupled transient gas flow calculation with a simultaneous calorific-value-gradient improved hydrogen tracking," *Appl. Energy*, vol. 316, Jun. 2022, Art. no. 118967.

[22] M. Chaczykowski, F. Sund, P. Zarodkiewicz, and S. M. Hope, "Gas composition tracking in transient pipeline flow," *J. Natural Gas Sci. Eng.*, vol. 55, pp. 321–330, Jul. 2018.

[23] G. Guandalini, P. Colbertaldo, and S. Campanari, "Dynamic modeling of natural gas quality within transport pipelines in presence of hydrogen injections," *Appl. Energy*, vol. 185, pp. 1712–1723, Jan. 2017.

[24] S. Pellegrino, A. Lanzini, and P. Leone, "Greening the gas network—The need for modelling the distributed injection of alternative fuels," *Renew. Sustain. Energy Rev.*, vol. 70, pp. 266–286, Apr. 2017.

[25] K. A. Pambour, R. Bolado-Lavin, and G. P. J. Dijkema, "An integrated transient model for simulating the operation of natural gas transport systems," *J. Natural Gas Sci. Eng.*, vol. 28, pp. 672–690, Jan. 2016.

[26] S. Zhang, W. Gu, S. Yao, S. Lu, S. Zhou, and Z. Wu, "Partitional decoupling method for fast calculation of energy flow in a large-scale heat and electricity integrated energy system," *IEEE Trans. Sustain. Energy*, vol. 12, no. 1, pp. 501–513, Jan. 2021.

[27] *PVWatts Calculator*, Nat. Renew. Energy Lab., Golden, CO, USA, May 2022.
[28] *Task Force C6.04.02: TB 575—Benchmark Systems for Network Integration of Renewable and Distributed Energy Resources*. Paris, France: CIGRÉ, 2014.
[29] G. Kerber, "Aufnahmefähigkeit von niederspannungsverteilnetzen für die einspeisung aus photovoltaikkleinanlagen," Ph.D. dissertation, Fachgebiet Elektrische Energieversorgungsnetze, Technische Universität München, München, 2011.
[30] C. Brosig, S. Fassbender, E. Waffenschmidt, S. Janocha, and B. Klaassen, "Benchmark gas distribution network for cross-sectoral applications," in *Proc. Int. Energy Sustainability Conf. (IESC)*, Piscataway, NJ, USA, Oct. 2017, pp. 1–5.
[31] M. Wolter, F. Beyrau, and E. Tsotsas, "Intelligentes multi-energie-system (SmartMES): Statusbericht der Otto-von-Guericke-Universität Magdeburg zum verbundprojekt," in *Res Electricae Magdeburgenses*, vol. 74. Magdeburg, Germany: Otto-von-Guericke-Universität, 2018.
[32] (May 12, 2022). *Solar Energy in the United States*. [Online]. Available: https://www.Energy.gov
[33] *Final 2021 Heating Electrification Forecast*, ISO New England, Holyoke, MA, USA, 2021.
[34] P. Gagnon, R. Margolis, J. Melius, C. Phillips, and R. Elmore, "Rooftop solar photovoltaic technical potential in the United States: A detailed assessment," Nat. Renew. Energy Lab., Golden, CO, USA, Tech. Rep. NREL/TP-6A20-65298, 2016.
[35] *Annual Energy Outlook 2022*, Energy Inf. Admin., Washington, DC, USA, May 2022.
[36] A. Christensen, "Assessment of hydrogen production costs from electrolysis: United States and Europe," Int. Council Clean Transp., Berlin, Tech. Rep., 2020.
[37] A. O. Oni, K. Anaya, T. Giwa, G. Di Lullo, and A. Kumar, "Comparative assessment of blue hydrogen from steam methane reforming, autothermal reforming, and natural gas decomposition technologies for natural gas-producing regions," *Energy Convers. Manage.*, vol. 254, Feb. 2022, Art. no. 115245.

JONTE DANCKER was born in Hamburg, Germany, in 1991. He received the B.Eng. degree in mechanical engineering from Baden-Wuerttemberg Cooperative State University Mannheim, Germany, in 2015, and the M.Sc. degree in sustainable energies from Otto von Guericke University Magdeburg (OVGU), Germany, in 2017.

He is currently a Scientific Assistant with the Chair Electric Power Networks and Renewable Energy, OVGU. His research interest includes integrated energy systems, their power flow calculation methods and optimization.

PABLO DUENAS MARTINEZ was born in Madrid, Spain, in 1984. He received the Ph.D. degree in electrical engineering from Universidad Pontificia Comillas, in 2013.

He is currently a Research Scientist with the Massachusetts Institute of Technology Energy Initiative, USA, and a Research Assistant Professor with Universidad Pontificia Comillas, Spain. His research interests include economic and regulatory modeling and analysis, and the role of traditional and new generation technologies in shaping the energy systems of the future, in low- to high-income countries and in a carbon-constrained world.

MARTIN WOLTER (Senior Member, IEEE) was born in Hannover, Germany, in 1981. He received the Diploma, Ph.D., and venia legendi degrees from Leibniz University Hannover, in 2006, 2008, and 2012, respectively.

He was the Head of the System Operation Concept Development Team, 50Hertz Transmission GmbH, for four years. Since 2015, he has been the Head of the Chair Electric Power Networks and Renewable Energy, Otto von Guericke University Magdeburg, Germany. His research interests include modeling and simulation of interconnected electric power systems, development of planning and operation strategies, and multi-agent systems.